

Strong frequency conversion in heterogeneously integrated GaAs resonators

Cite as: APL Photonics 4, 036103 (2019); <https://doi.org/10.1063/1.5065533>

Submitted: 11 October 2018 . Accepted: 27 February 2019 . Published Online: 15 March 2019

Lin Chang, Andreas Boes , Paolo Pintus , Jon D. Peters, MJ Kennedy, Xiao-Wen Guo, Nicolas Volet, Su-Peng Yu, Scott B. Papp, and John E. Bowers

COLLECTIONS

 This paper was selected as an Editor's Pick



View Online



Export Citation



CrossMark

ARTICLES YOU MAY BE INTERESTED IN

[On the observation of dispersion in tunable second-order nonlinearities of silicon-rich nitride thin films](#)

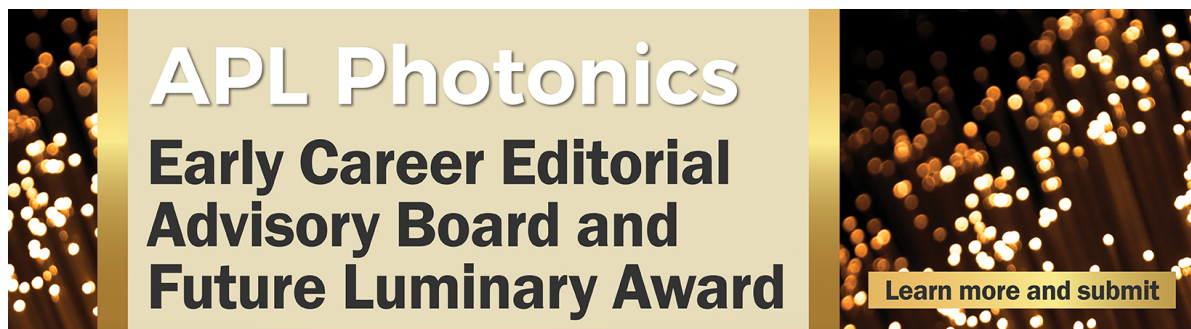
APL Photonics 4, 036101 (2019); <https://doi.org/10.1063/1.5053704>

[On-chip dynamic time reversal of light in a coupled-cavity system](#)

APL Photonics 4, 030806 (2019); <https://doi.org/10.1063/1.5080359>

[Adiabatic mode converters for silicon photonics: Power and polarization broadband manipulators](#)

APL Photonics 4, 030803 (2019); <https://doi.org/10.1063/1.5080247>



APL Photonics
**Early Career Editorial
Advisory Board and
Future Luminary Award**

[Learn more and submit](#)

Strong frequency conversion in heterogeneously integrated GaAs resonators

Cite as: APL Photon. 4, 036103 (2019); doi: 10.1063/1.5065533

Submitted: 11 October 2018 • Accepted: 27 February 2019 •

Published Online: 15 March 2019



View Online



Export Citation



CrossMark

Lin Chang,^{1,a)} Andreas Boes,^{1,2}  Paolo Pintus,¹  Jon D. Peters,¹ MJ Kennedy,¹ Xiao-Wen Guo,¹ Nicolas Volet,¹ Su-Peng Yu,³ Scott B. Papp,³ and John E. Bowers¹

AFFILIATIONS

¹Department of Electrical and Computer Engineering, University of California, Santa Barbara, California 93106, USA

²School of Engineering, RMIT University, Melbourne, VIC 3000, Australia

³Time and Frequency Division, National Institute of Standards and Technology, Boulder, Colorado 80305, USA

^{a)}Electronic mail: linchang@ucsb.edu.

ABSTRACT

In this contribution, we demonstrate the first integrated gallium arsenide (GaAs) ring resonator for second harmonic generation (SHG) on a GaAs-on-insulator platform. Such resonators exhibit high nonlinear optical coefficients, a strong optical confinement, and intrinsic quality factors exceeding 2.6×10^5 , which makes them very attractive for nonlinear optical applications. The fabricated resonators exhibit a great potential for frequency conversion: when $61 \mu\text{W}$ of pump power at $2 \mu\text{m}$ wavelength is coupled into the cavity, the absolute internal conversion efficiency is 4%. We predict an external SHG efficiency beyond 1 000 000%/W based on the GaAs resonance devices. Such nonlinear resonant devices of GaAs and its aluminum GaAs alloy can be directly integrated with active components in nonlinear photonic integrated circuits (PICs). This work paves a way for ultra-high efficient and compact frequency conversion elements in PICs.

© 2019 Author(s). All article content, except where otherwise noted, is licensed under a Creative Commons Attribution (CC BY) license (<http://creativecommons.org/licenses/by/4.0/>). <https://doi.org/10.1063/1.5065533>

The second-order nonlinearity ($\chi^{(2)}$) is one of the most important material properties in nonlinear optics and has been applied to a broad range of applications. In quantum optics, the second-order nonlinearity is often used for generating entangled photon pairs by spontaneous parametric down-conversion (SPDC)¹ and for providing continuous variable entanglement in an optical parametric oscillator (OPO) configuration.² In classical photonics, it plays key roles in various applications such as nonlinear microscopy, optical frequency references, and light source at various wavelength, among others.^{3,4} Recently, there has been a tremendous interest in integrating those nonlinear components into photonic integrated circuits (PICs), which will miniaturize the nonlinear optical system, significantly reduce the cost and power consumption, and dramatically improve the system performance.⁵⁻¹⁰

However, big challenges remain in order to achieve that goal. First, the power levels that are achievable with integrated lasers are usually not high enough to drive current on-chip nonlinear optical processes efficiently. Typical on-chip laser powers are in the order of tens of milliwatt or lower.¹¹ However, most demonstrated

integrated $\chi^{(2)}$ nonlinear devices do not meet the efficiency requirements to work at these power levels. One example is OPOs. So far the lasing of an integrated OPO based on $\chi^{(2)}$ nonlinearity, which is pumped by an on-chip laser, has not been demonstrated due to the high threshold power requirements.¹² Another difficulty is that most $\chi^{(2)}$ materials used for PICs are not compatible with the integrated active devices, either in design, fabrication, or integration. As a result, the nonlinear components are still far from being integrated together with lasers, amplifiers, and photodetectors on the same chip but have to be connected by either fiber coupling or chip to chip butt coupling. This dilemma not only drops the conversion efficiency of the nonlinear optical process by orders of magnitude due to the power lost in coupling but also introduces degradation to the whole system performance due to the coupling instabilities and reflections of the facets.

We believe that the key to solve this problem is to find materials that can be used for ultra-high efficient nonlinear processes and as active devices simultaneously. Recently, GaAs on insulator and its closely related aluminum gallium arsenide (AlGaAs) alloy have

drawn a lot of attention as a platform for nonlinear optical applications on chips.^{13–19} Those platforms are very attractive as GaAs (AlGaAs) has one of the highest nonlinear optical coefficients, both $\chi^{(2)}$ and $\chi^{(3)}$, among commonly used waveguide materials.¹³ Importantly, the waveguides have a high refractive index contrast, which enables high intensities at moderate powers due to the strongly confined optical waveguide mode, and thus further enhances the nonlinear optical efficiency. Besides these, another key advantage of GaAs (AlGaAs), which distinguishes them from other nonlinear materials, is that they and their alloys (InGaAs, InGaAsP, etc.) are efficient light sources in PICs.¹¹ This provides a great opportunity to combine nonlinear optical elements and laser pump sources on the same platform.

Recently, we demonstrated a record of high second harmonic generation (SHG) normalized efficiency of 13 000% $W^{-1} \text{ cm}^{-2}$ in straight waveguides based on the GaAs on an insulator platform.¹³ This efficiency is one order of magnitude higher than those of previous SHG devices.⁵ Creating a resonance structure in this platform is the next important step to harness the extraordinary nonlinear performance because even higher nonlinear optical conversion efficiencies are expected compared to straight waveguides, due to the power built up inside the cavities. Previously, GaAs (AlGaAs) microdisk resonators for SHG have been demonstrated on native substrates by undercutting the sacrificial layers,^{20,21} but their conversion efficiencies are limited by the relative low quality factors, which are usually less than 10^5 . Furthermore, those devices were incompatible with the integration of other photonic components on the same platform. Both of these problems can be overcome with the platform in this work, due to the low propagation loss of waveguides $< 2 \text{ dB/cm}$ ($> 2 \times 10^5$ quality factor)¹³ and compatibility with wafer scale integration.

In this work, we investigate ring resonators in GaAs on an insulator for SHG at a wavelength of $2 \mu\text{m}$, to show the potential of GaAs (AlGaAs) resonance structures for highly efficient frequency conversion. Low loss waveguides enable ring resonators with an intrinsic quality factor of $\sim 2.6 \times 10^5$ at a wavelength of $2 \mu\text{m}$. The strong power enhancement inside the cavity, in combination with the high nonlinear coefficient and small mode volume, leads to a significant pump power depletion at sub-milliwatt power levels. We estimate that around 4% of the $61 \mu\text{W}$ pump power coupled into the cavity is frequency doubled. Furthermore, we predict a SHG external efficiency beyond 1 000 000% W^{-1} based on the GaAs resonance devices. This work paves the way for ultra-high efficient and compact nonlinear devices and for future integration of nonlinear components and active devices in the same PIC platform.

The cross section of the nonlinear optical waveguide is illustrated in Fig. 1(a), where the waveguide core material ($\langle 001 \rangle$ oriented GaAs) is fully surrounded by silica. We choose a SHG process in the GaAs waveguide between TE-polarized pump light and TM polarized second harmonic (SH) light,¹³ determined by the non-zero susceptibility elements of the $\chi^{(2)}$ tensor. One of the key requirements for high-efficiency SHG is the phase match condition, which in $\langle 001 \rangle$ oriented GaAs ring resonators can be fulfilled by^{20,22}

$$|2m_P - m_{SH}| = 2, \quad (1)$$

where m_P and m_{SH} correspond to the azimuthal numbers of pump and SH light, respectively. The azimuthal number follows the relation

$$\omega_{P,SH} \times n_{P,SH} / c = m_{P,SH} / R, \quad (2)$$

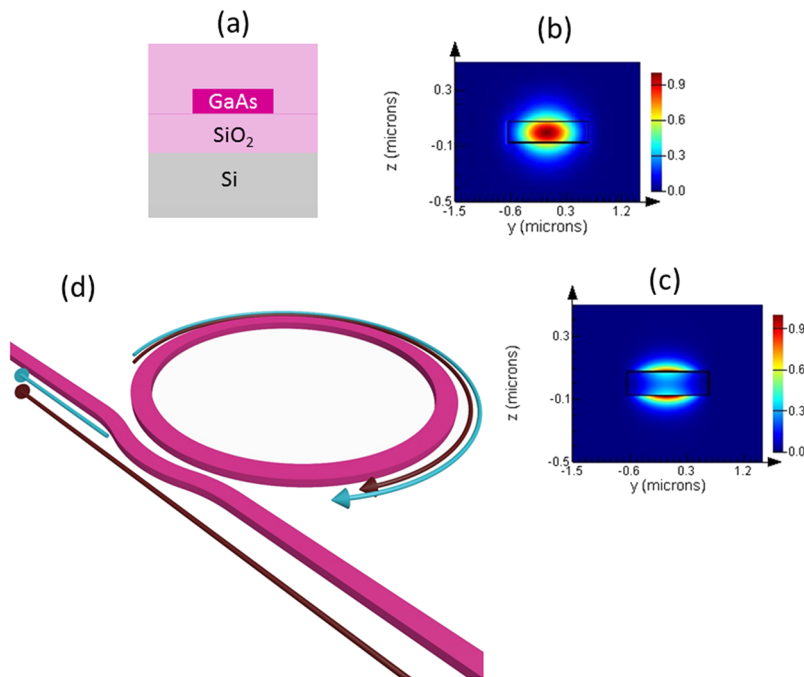


FIG. 1. (a) Cross section of GaAs on an insulator waveguide; (b) and (c) electric field distributions for fundamental TE mode at a wavelength of $2 \mu\text{m}$ and TM mode at a wavelength of $1 \mu\text{m}$; and (d) schematic structure of the ring resonator with a pulley coupler.

where $\omega_{p,SH}$ are the frequencies of pump and SH light, $n_{p,SH}$ are the effective indices of modes at those two frequencies, and R is the radius of the ring resonator. From Eqs. (1) and (2), the relations between n_p and n_{SH} can be obtained,

$$n_{SH} = \left(1 \pm \frac{1}{m_p}\right)n_p. \quad (3)$$

This relation indicates that, compared to the modal phase match used in the straight waveguide, where n_p and n_{SH} should be exactly matched, here we have an offset factor of $1/m_p$ between the indices at two wavelengths. In this work, the radius of the resonator we used is $100 \mu\text{m}$, which correspond to an m_p value around 650 and m_{SH} around 1300 ± 2 . As a result, $1/m_p$ is much lower than 1, which means that we can design the waveguide geometry to match the two indices very closely, similar for the case of the straight waveguide. Here we pick the waveguide of the resonator to be 150 nm thick and 1300 nm wide, which corresponds to a phase match wavelength of $\sim 2 \mu\text{m}$. The profiles of the TE mode at a wavelength of $2 \mu\text{m}$ and TM mode at a wavelength of $1 \mu\text{m}$ are shown in Figs. 1(c) and 1(d), respectively.

The ring resonator is coupled to the bus waveguide with a pulley coupler, as illustrated in Fig. 1(d). The width of the bus waveguide is 900 nm , and the gap between the bus and ring waveguides is 200 nm . These geometries mean that the resonator is highly undercoupled for both wavelengths. To achieve the highest external conversion efficiency of the resonator, one ideally has both wavelengths critically coupled.²³ However, increasing the coupling requires that either the coupling length is increased or the gap-size is reduced between the waveguides. We did not pursue either option as a longer coupling length will impact the phase matching condition in the resonator and the gap-size was limited by the lithography step used to define the waveguides.

The fabrication process of the GaAs waveguide is illustrated in Fig. 2. The GaAs film is integrated onto a Si wafer with $3 \mu\text{m}$ SiO₂ top cladding by wafer bonding. After removal of the GaAs native substrate, the GaAs thin-film is patterned by Deep Ultraviolet (DUV) lithography and dry etching. Details of the process can be found in Ref. 13. Compared to the previous integration technology

for $\chi^{(2)}$ materials on chip, which are done by either ion-slicing²⁴ or direct deposition, e.g., sputtering,⁸ the use of metalorganic chemical vapor deposition (MOCVD) (MBE) has the advantage that single crystal GaAs thin-films can be grown with a thickness control of 1 nm over centimeter length scales.¹³ Those are key requirements for $\chi^{(2)}$ nonlinear processes in order to control the phase matching wavelength.

Experimentally, we characterized the devices by coupling pump light with a wavelength of around $2 \mu\text{m}$ into the bus waveguide and detect the transmitted power at the pump and SHG wavelength after splitting them using a wavelength demultiplexer. Figure 3(a) shows the wavelength response of the ring resonator for the pump light and the corresponding SH light inside the bus waveguide as a function of the pump wavelength. Based on the full width at half maximum (FWHM) (8 pm) of the fitted resonance [see the inset in Fig. 3(a)] at the pump wavelength, we estimate the intrinsic quality factor of the ring resonator to be higher than 2.6×10^5 around $2 \mu\text{m}$ wavelength. This corresponds to a linear propagation loss of below 2 dB/cm . A measurement with a finer spectral resolution is currently limited by the wavelength step size of our laser. The quality factor at $1 \mu\text{m}$ is estimated to be around 5.7×10^4 , based on the propagation loss extracted from cutback measurement.

Figure 3(a) also shows that the SH power is only detected at the resonance of the pump light. The pump power P_p and SHG power P_{SH} inside the bus waveguide are estimated based on the waveguide to fiber coupling coefficients at the chip facets of 56% and 12.6% , respectively. The coupling structures are the inverse tapers designed for $2\text{-}\mu\text{m}$ light. The design of more efficient edge couplers at the SHG wavelength can be realized by using EBL lithography in the future, in which case the coupling coefficient is expected to be higher than 60% . The inset of Fig. 3(b) shows the P_{SH} as a function of P_p . The red dashed line has a slope of 2 in dB scale, which corresponds to the case of having no pump power depletion. The green dots represent the experimental results, where the deviation from the red line occurs at a pump power of less than 1 mW inside the bus waveguide, of which $<200 \mu\text{W}$ power is coupled into the resonator. This indicates that a significant frequency conversion takes place inside the cavity at very low pump powers as the pump gets depleted.

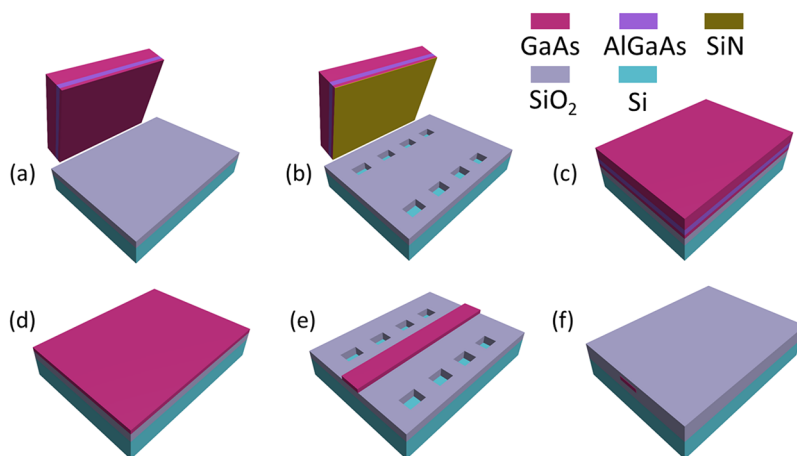


FIG. 2. Processing flow for the GaAs on insulator waveguide fabrication.

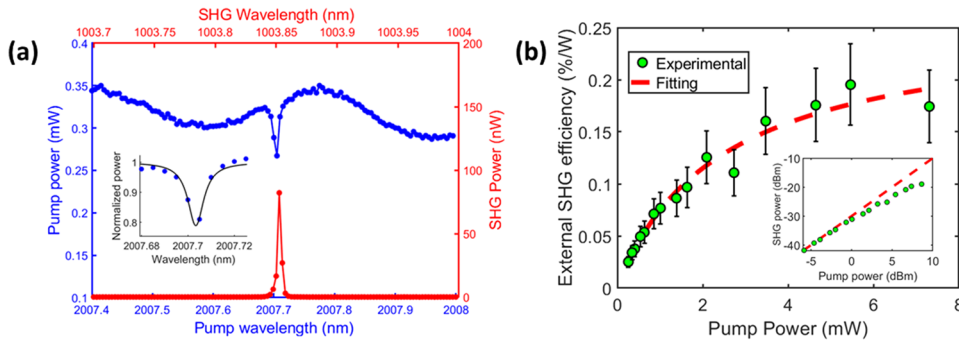


FIG. 3. Experimental results and analysis: (a) pump and SHG spectrum for the ring resonator; the embedded figure shows the zoomed in resonance and fitting curve; (b) dependence of external SHG conversion efficiency on the pump power, experimental results and calculation from Eq. (5); the embedded figure shows the SHG power as a function of the pump power; experimental results are compared to the case of no depletion (red dashed line).

The external normalized SHG efficiency for this device is around 100%/W at the low pump power region, which is orders of magnitude higher compared to the efficiency of previous research on GaAs (AlGaAs) microdisks.^{20,21} When one considers that the ring resonator is highly under-coupled at both pump and SHG wavelengths, the internal conversion efficiency is a better parameter for characterizing the cavity’s capability for frequency conversion. Here the internal efficiency refers to SHG efficiency inside the cavity. To extract that, we consider the following equations describing the SHG process inside the resonator:²³

$$X(1 + X)^2 = \frac{r_P}{1 + r_P} \frac{P_P}{P_0}, \quad (4)$$

$$\eta_{SH} = \frac{P_{SH}}{P_P} = 4 \frac{r_{SH}}{1 + r_{SH}} \frac{r_P}{1 + r_P} \frac{X}{(1 + X)^2}, \quad (5)$$

$$r_{P,SH} = \kappa_{P,SH}^2 / \alpha_{P,SH}, \quad (6)$$

where $t_{P,SH}$ and $\kappa_{P,SH}$ are the transmission and coupling coefficients of the coupler, $\alpha_{P,SH}$ is the roundtrip loss of the cavity, X is the intracavity power normalized to P_0 , and η_{SH} refers to the external SHG conversion efficiency. By combining Eqs. (4) and (5), the correlation between η_{SH} and P_P can be built, with two unknown constants r_{SH} and P_0 . P_0 is the characteristic power constant indicating the point higher than which the depletion starts to be significant. The value of r_P can be extracted from the spectrum of pump resonance.

Figure 3(b) shows the plot of η_{SH} as a function of P_P . By fitting Eqs. (4) and (5) based on the experimental results (green dots), we extracted the values of r_{SH} and P_0 to be 0.05 and 0.4 mW, respectively, which correspond to the red dashed curve. It can be seen that the experimental results match well with the theory. Here, we did not include the nonidealities of the cavity into our model, which will be discussed afterwards.

The following equation is used to estimate how much of the pump power that is coupled into the cavity is frequency doubled,

$$\eta_{SH,in} = \frac{1 + r_{SH}}{r_{SH}} \frac{P_{SH}}{P_P - P_{P,t}}, \quad (7)$$

where $P_{P,t}$ is the transmitted power of pump light, which can be determined by our experimental results. When there is 0.34 mW pump power inside the bus waveguide, 61 μ W of it is coupled into cavity. The internal conversion efficiency in this situation is estimated to be 4% based on Eq. (7), which correspond to an internal

normalized efficiency around 65 000%/W. Such a high internal conversion efficiency can be explained by the high nonlinear optical coefficients of GaAs compared to those of other $\chi^{(2)}$ resonators, the tight mode confinement, the efficient phase-matching, and the high quality factors we achieved in this platform. However, we need to point out that the internal conversion efficiency cannot be fully utilized for external SHG applications,²⁵ but it indicates the potential of this resonator for $\chi^{(2)}$ -based nonlinear processes.

To extract the external conversion efficiency for our device at critical coupling, we consider the expression for the characteristic power P_0 , derived from Eqs. (4)–(6),

$$P_0 = v_P \frac{\pi \epsilon_0 n_P^4 n_{SH}^2}{8d^2} \frac{1}{Q_{oP}^2 Q_{oSH}} \frac{V_P^2 V_{SH}}{V_{PPSH}^2} (1 + r_P)^2 (1 + r_{SH}) = B(1 + r_P)^2 (1 + r_{SH}), \quad (8)$$

where B is a constant. In the low pump power region, Eq. (4) becomes $X = A$, because $X \gg X^2 \gg X^3$. Then by combining Eqs. (4), (5), and (8), we obtain the external conversion efficiency to be

$$\eta_{SH} = 4 \frac{r_{SH}}{(1 + r_{SH})^2} \left(\frac{r_P}{(1 + r_P)} \right)^2 \frac{P_P}{B} = \eta_{SH,Nor} P_P. \quad (9)$$

When $r_{SH} = r_P = 1$, the external normalized conversion efficiencies under low pump powers have the maximum values, which correspond to the critical coupling condition for both the pump and the SH wavelength. Based on the experimental results, r_P and r_{SH} of the devices are extracted to be 0.053 and 0.050, respectively. P_0 is extracted to be 0.4 mW. Thus B is estimated to be 0.34 mW.

By plugging the value of B and $r_{SH} = r_P = 1$ into Eq. (9), the external normalized conversion efficiency at critical coupling for the current device is estimated to be 18 400%/W. This is about 4 times lower than the calculated value (68 445%/W) in the ideal case (see the Appendix). A possible reason for this discrepancy may be due to the uniformity or defects inside the cavities. Another factor which may also affects the efficiency is the mismatch between resonances, either caused by the initial structure of the ring or the thermal effect when injecting high power into the cavity. According to Ref. 8, when taking the resonance detuning into consideration, Eq. (9) becomes

$$\eta_{SH} = 4 \frac{r_{SH}}{\delta_{SH}^2 + (1 + r_{SH})^2} \left(\frac{r_P}{\delta_P^2 + (1 + r_P)^2} \right)^2 \frac{P_P}{B}. \quad (10)$$

Here $\delta_p = (\omega_{p,r} - \omega_p)/\alpha_p$ ($\delta_{SH} = (\omega_{SH,r} - 2\omega_p)/\alpha_{SH}$), where $\omega_{p,r}$ and $\omega_{SH,r}$ correspond to the resonances of pump and SHG frequency, respectively. $\delta_p = 0$ because the pump wavelength at which we extracted the efficiency is very close to the resonance, as shown in Fig. 3(a). δ_{SH} indicates the mismatch between SHG wavelength and the resonance. The conversion efficiency reaches the maximum when both pump and SHG wavelength are perfectly resonate and drops significantly when the mismatch between two resonance increases. The power built up in the cavity may cause a strong thermal optic effect to shift the resonances, which may influence the conversion efficiency under different pump powers. In this experiment, at low pump power levels where the highest conversion efficiency is extracted, we did not observe an obvious thermal shift of the resonance. When the pump power was increased, the thermal shift could be observed and the pump wavelength was adjusted to follow it, whose maximum value ($\Delta\omega_{p,r}$) at the highest power level is $2\pi \times 6.4$ GHz. Assuming that the dependences of resonance shifts on temperature are similar with results in Ref. 21, where $(2\Delta\omega_p)/(\Delta\omega_{SH} - 2\Delta\omega_p) = 0.077/(0.083 - 0.077) = 12.8$, we estimate the value of δ_{SH} to be ~ 0.1 . Then by plugging δ_{SH} into Eq. (10), the maximum drop of the efficiency caused by the thermal effect in this work is less than 1%.

Another factor that can potentially influence the efficiency is the nonlinear loss. According to Ref. 26, the two photon absorption (2PA) of GaAs at $2 \mu\text{m}$ is negligible, and the three photon absorption (3PA) is $\sim 2 \text{ cm}^3/\text{GW}^2$, which leads to a nonlinear loss less than 0.001 dB/cm inside the cavity under the highest power level in our experiment. This indicates that here the nonlinear loss is not a main contributor to the drop of efficiencies compared to other factors. However, for the nonlinear applications pumped at the wavelength below $1.8 \mu\text{m}$, GaAs will have a strong 2PA loss. In that case, using AlGaAs with larger bandgap will be a better option. Furthermore, one also needs to keep in mind that GaAs can form a native oxide layer at the surface during processing, which can form interface states within the bandgap, causing additional losses.²⁷ Such losses can be reduced by appropriate surface passivation.²⁸

To further improve the conversion efficiency, a race track resonator will be a better choice compared to the ring resonators as the phase matching condition can truly be fulfilled along the straight waveguides rather than relying on the quasi-phase matching approach in a ring resonator. If the straight section is much longer than the curved section and aligned to the direction where the SHG interaction corresponds to the non-zero susceptibility elements of the $\chi^{(2)}$ tensor, we can treat the resonator with a constant nonlinear coefficient d_{14} . For such a resonator with 1 mm perimeter, at $2 \mu\text{m}$ pump wavelength, $\nu_p = 150$ THz, $n_{p,SH} = 2.2$, $d_{14} = 104 \text{ pm/V}$, $Q_{0p} = 2.6 \times 10^5$, $Q_{0SH} = 5.7 \times 10^4$, and $V_p^2 V_{SH}/V_{PPSH}^2 = 2400 \mu\text{m}^3$ and assuming $r_{p,SH} = 1$, we estimate the normalized external efficiency at the low power region to be 1 830 000%/W based on Eqs. (8) and (9).

This strong frequency conversion indicates the great potential for resonators on this platform for on-chip nonlinear applications. A significant amount of power can be converted to the second harmonic wavelength even with a pump power below 1 mW. These properties can make many currently inaccessible on-chip nonlinear systems with limited power budget possible, such as the on-chip self-reference of the frequency comb,²⁹ in which the pump power of

the comb teeth for frequency doubling is around $10 \mu\text{W}$. For optical parametric oscillators (OPOs), the resonance structures will lead to an ultralow threshold at several micro-watts, which can readily be satisfied by the current integrated lasers and will also bring huge benefits to quantum applications as the filtering requirements of the pump power can be relaxed.³⁰

In addition to the $\chi^{(2)}$ -based nonlinear process, the GaAs (AlGaAs) resonators with a high quality factor can also play important roles in $\chi^{(3)}$ -based applications,¹⁴ because of the extremely high third order nonlinear coefficient, small mode volume, and anomalous dispersions which can be achieved by tailoring the waveguide geometry. According to our calculations, at 1550 nm wavelength, for a 1-THz resonator for frequency generation, the threshold is around 0.5 mW based on the current quality factor we achieved. We believe it is possible to reduce the propagation loss of the waveguide and increase the quality factor of resonator by optimizing our fabrication process. With a 1×10^6 intrinsic quality factor, the threshold can be reduced further down to $30 \mu\text{W}$.

In conclusion, we demonstrate the first integrated GaAs on insulator ring resonator that utilized the second-order nonlinearity. Based on this, 4% frequency doubling inside a ring resonator is observed when $61 \mu\text{W}$ pump power at a wavelength of $2 \mu\text{m}$ is coupled into the cavity. An external SHG conversion efficiency beyond 1 000 000%/W has been predicted based on GaAs resonance structures. The GaAs resonators, along with the similar AlGaAs resonance structures, provide not only a route to achieve extremely high efficiency frequency conversion but also an attractive solution to combine active and nonlinear devices in the same PIC platform. Furthermore, this platform enables studies of classical nonlinear optics in extreme regimes and the potential for generation and processing of quantum information by extreme nonlinearities.

This work was funded by DARPA MTO DODOS Contract (No. HR0011-15-C-055). We thank Daehwan Jung, Justin Norman, Tony Huang, Minh Tran, Tin Komljenovic, Alfredo Torres, and Alexander Spott for valuable discussions and fabrication help. We would also like to thank Scott Diddams, Richard Mirin, Martin Fejer, Carsten Langrock, and Alireza Marandi for fruitful discussions. N.V. acknowledges support from the Swiss National Science Foundation.

APPENDIX: CALCULATION FOR SHG EFFICIENCY IN IDEAL GaAs RESONATORS

This part describes the theory of SHG conversion efficiencies in ideal GaAs ring resonators.

To calculate the ideal conversion efficiency for a GaAs ring resonator, it is hard to use Eq. (8) directly as d is not a constant value for a ring resonator due to waveguide bends. In Ref. 31, a detailed theoretical analysis has been done to deal with this problem, which will be referred to in the following.

In the low pump power region, for an ideal GaAs ring resonator, with critical couples and aligned resonances, the expected SHG power coupled outside the resonator is

$$P_{SH} = (P_p)^2 (1 - |t_{SH}|^2) \frac{|2\pi K_{\pm}|^2 \alpha_{SH}^2}{(1 - \alpha_{SH} |t_{SH}|)^2} \left(\frac{\alpha_f^2 (1 - |t_f|^2)}{(1 - \alpha_f |t_f|)^2} \right)^2, \quad (\text{A1})$$

where K_{\pm} is the nonlinear coupling coefficients for $\Delta m = \pm 2$. In a cylindrical coordination system, it can be expressed as

$$K_{\pm} = \mp \frac{d_{14}}{2\epsilon_0\omega_0 n_p^4} \int_{-\frac{h}{2}}^{\frac{h}{2}} \tilde{Z}_{SH}(z) \tilde{Z}_P^2(z) dz \times \dots \times \int_{-\frac{w}{2}}^{\frac{w}{2}} r \tilde{\psi}_{SH} \left(\frac{m_P}{r} \tilde{\psi}_P \pm \frac{\partial \psi_P}{\partial r} \right)^2 dr, \quad (\text{A2})$$

where $\Psi(r)$ and $Z(z)$ come from the expression for the field distribution ($F_z = H_z$ or E_z) of the mode,

$$F_z \exp(i\omega t) = A(\theta) \psi(r) Z(z) \exp[i(\omega t - m\theta)]. \quad (\text{A3})$$

For more details, refer to Ref. 31. Here, we solve the modes numerically by using Lumerical finite-difference time domain (FDTD). Then through Eq. (A2) we obtain the value of K_+ and K_- to be $0.0575 \text{ W}^{-1/2}$ and $0.042 \text{ W}^{-1/2}$, respectively. The external normalized conversion efficiencies are estimated to be $68.445\%/W$ and $36.504\%/W$, respectively, which are about four times higher than the values we estimated above.

REFERENCES

- ¹X. Guo, C. L. Zou, C. Schuck, H. Jung, R. Cheng, and H. X. Tang, *Light: Sci. Appl.* **6**, e16249 (2017).
- ²U. L. Andersen, T. Gehring, C. Marquardt, and G. Leuchs, *Phys. Scr.* **91**(5), 053001 (2016).
- ³X. Chen, O. Nadiarynk, S. Plotnikov, and P. J. Campagnola, *Nat. Protoc.* **7**, 654 (2012).
- ⁴J. E. Bowers, A. Beling, D. Blumenthal, A. Bluestone, S. M. Bowers, T. C. Briles, L. Chang, S. A. Diddams, G. Fish, H. Guo, T. J. Kippenberg, T. Komljenovic, E. Norberg, S. Papp, M. H. P. Pfeiffer, K. Srinivasan, L. Theogarajan, K. J. Vahala, and N. Volet, in *2016 IEEE International Frequency Control Symposium (IFCS)* (IEEE, 2016).
- ⁵L. Chang, Y. Li, N. Volet, L. Wang, J. Peters, and J. E. Bowers, *Optica* **3**, 531 (2016).
- ⁶A. Boes, B. Corcoran, L. Chang, J. Bowers, and A. Mitchell, *Laser Photonics Rev.* **12**, 1700256 (2018).
- ⁷I. Roland, M. Gromovyi, Y. Zeng, M. El Kurdi, S. Sauvage, C. Brimont, T. Guillet, B. Gayral, F. Semon, J. Y. Duboz, M. De Micheli, X. Chécoury, and P. Boucaud, *Sci. Rep.* **6**, 34191 (2016).
- ⁸X. Guo, C.-L. Zou, and H. X. Tang, *Optica* **3**, 1126 (2016).
- ⁹L. Chang, M. H. P. Pfeiffer, N. Volet, M. Zervas, J. D. Peters, C. L. Manganelli, E. J. Stanton, Y. Li, T. J. Kippenberg, and J. E. Bowers, *Opt. Lett.* **42**, 803 (2017).
- ¹⁰C. Wang, C. Langrock, A. Marandi, M. Jankowski, M. Zhang, B. Desiatov, M. M. Fejer, and M. Loncar, in *Conference on Lasers and Electro-Optics (OSA, Washington, DC, 2018)*, p. JTh5A.2.
- ¹¹T. Komljenovic, M. Davenport, J. Hulme, A. Liu, C. Santis, A. Spott, S. Srinivasan, E. Stanton, C. Zhang, and J. Bowers, *J. Lightwave Technol.* **34**, 20 (2015).
- ¹²M. Savanier, A. Andronico, X. Lafosse, P. Filloux, I. Favero, S. Ducci, and G. Leo, in *CLEO Science and Innovations* (Optical Society of America, 2012), p. JW4A.66.
- ¹³L. Chang, A. Boes, X. Guo, D. T. Spencer, M. Kennedy, J. D. Peters, N. Volet, J. Chiles, A. Kowligy, N. Nader, D. D. Hickstein, E. J. Stanton, S. A. Diddams, S. B. Papp, and J. E. Bowers, *Laser Photonics Rev.* **12**, 1870044 (2018).
- ¹⁴M. Pu, L. Ottaviano, E. Semenova, and K. Yvind, *Optica* **3**, 823 (2016).
- ¹⁵N. Morais, I. Roland, M. Ravano, W. Hease, A. Lemaitre, C. Gomez, S. Wabnitz, M. De Rosa, I. Favero, and G. Leo, *Opt. Lett.* **42**, 4287 (2017).
- ¹⁶A. Fiore, V. Berger, E. Rosencher, P. Bravetti, and J. Nagle, *Nature* **391**, 463 (1998).
- ¹⁷L. Scaccabarozzi, M. M. Fejer, Y. Huo, S. Fan, X. Yu, and J. S. Harris, *Opt. Lett.* **31**, 3626 (2006).
- ¹⁸T. Matsushita, Y. Nakamura, S. Matsumoto, T. Onda, I. Shoji, and T. Kondo, in *2013 Conference on Lasers Electro-Optics Pacific Rim (IEEE, 2013)*, pp. 1–2.
- ¹⁹M. Savanier, C. Ozanam, L. Lanco, X. Lafosse, A. Andronico, I. Favero, S. Ducci, and G. Leo, *Appl. Phys. Lett.* **103**, 261105 (2013).
- ²⁰P. S. Kuo, J. Bravo-Abad, and G. S. Solomon, *Nat. Commun.* **5**, 3109 (2014).
- ²¹S. Mariani, A. Andronico, A. Lemaitre, I. Favero, S. Ducci, and G. Leo, *Opt. Lett.* **39**, 3062 (2014).
- ²²Y. Dumeige and P. Féron, *Phys. Rev. A* **74**, 063804 (2006).
- ²³I. Breunig, *Laser Photonics Rev.* **10**, 569 (2016).
- ²⁴L. Chen, J. Nagy, and R. M. Reano, *Opt. Mater. Express* **6**, 2460 (2016).
- ²⁵S. Khripunov, S. Kobtsev, and D. Radnatarov, *Appl. Opt.* **55**, 502 (2016).
- ²⁶W. C. Hurlbut, Y.-S. Lee, K. L. Vodopyanov, P. S. Kuo, and M. M. Fejer, *Opt. Lett.* **32**, 668 (2007).
- ²⁷D. Parrain, C. Baker, G. Wang, B. Guha, E. G. Santos, A. Lemaitre, P. Senellart, G. Leo, S. Ducci, and I. Favero, *Opt. Express* **23**, 19656 (2015).
- ²⁸B. Guha, F. Marsault, F. Cadiz, L. Morgenroth, V. Ulin, V. Berkovitz, A. Lemaitre, C. Gomez, A. Amo, S. Combrié, B. Gérard, G. Leo, and I. Favero, *Optica* **4**, 218 (2017).
- ²⁹D. T. Spencer, T. Drake, T. C. Briles, J. Stone, L. C. Sinclair, C. Fredrick, Q. Li, D. Westly, B. R. Ilic, A. Bluestone, N. Volet, T. Komljenovic, L. Chang, S. H. Lee, D. Y. Oh, M. G. Suh, K. Y. Yang, M. H. P. Pfeiffer, T. J. Kippenberg, E. Norberg, L. Theogarajan, K. Vahala, N. R. Newbury, K. Srinivasan, J. E. Bowers, S. A. Diddams, and S. B. Papp, *Nature* **557**, 81 (2018).
- ³⁰N. C. Harris, D. Grassani, A. Simbula, M. Pant, M. Galli, T. Baehr-Jones, M. Hochberg, D. Englund, D. Bajoni, and C. Galland, *Phys. Rev. X* **4**, 041047 (2014).
- ³¹P. S. Kuo and G. S. Solomon, *Opt. Express* **19**, 16898 (2011).